

Research Article

$K^0 - \bar{K}^0$ Mixing in the Minimal Flavor-Violating Two-Higgs-Doublet Models

Natthawin Cho, Xin-Qiang Li, Fang Su, and Xin Zhang

Institute of Particle Physics and Key Laboratory of Quark and Lepton Physics (MOE), Central China Normal University, Wuhan, Hubei 430079, China

Correspondence should be addressed to Fang Su; sufang@itp.ac.cn

Received 14 May 2017; Accepted 10 July 2017; Published 29 August 2017

Academic Editor: Alexey A. Petrov

Copyright © 2017 Natthawin Cho et al. This is an open access article distributed under the Creative Commons Attribution License, which permits unrestricted use, distribution, and reproduction in any medium, provided the original work is properly cited. The publication of this article was funded by SCOAP³.

The two-Higgs-doublet model (2HDM), as one of the simplest extensions of the Standard Model (SM), is obtained by adding another scalar doublet to the SM and is featured by a pair of charged Higgs, which could affect many low-energy processes. In the “Higgs basis” for a generic 2HDM, only one scalar doublet gets a nonzero vacuum expectation value and, under the criterion of minimal flavor violation, the other one is fixed to be either color-singlet or color-octet, which are named as type III and type C 2HDM, respectively. In this paper, we study the charged-Higgs effects of these two models on the $K^0 - \bar{K}^0$ mixing, an ideal process to probe New Physics (NP) beyond the SM. Firstly, we perform a complete one-loop computation of the box diagrams relevant to the $K^0 - \bar{K}^0$ mixing, keeping the mass and momentum of the external strange quark up to the second order. Together with the up-to-date theoretical inputs, we then give a detailed phenomenological analysis, in the cases of both real and complex Yukawa couplings of the charged Higgs to quarks. The parameter spaces allowed by the current experimental data on the mass difference Δm_K and the CP-violating parameter ϵ_K are obtained and the differences between these two 2HDMs are investigated, which are helpful to distinguish them from each other from a phenomenological point of view.

1. Introduction

The SM of particle physics has been proved to be successful because of its elegance and predictive capability. Almost all predictions in the SM are in good agreement with the experimental measurements, especially for the discovery of a Higgs boson with its mass around 125 GeV [1, 2]. The discovery of a SM-like Higgs boson suggests that the electroweak symmetry breaking (EWSB) is probably realized by the Higgs mechanism implemented via a single scalar doublet. However, the EWSB is not necessarily induced by just one scalar. It is interesting to note that many NP models are equipped with an extended scalar sector; for example, the minimal supersymmetric standard model requires at least two Higgs doublets [3]. Moreover, the SM does not provide enough sources of CP violation to generate the sufficient size of baryon asymmetry of the universe (BAU) [4–6].

One of the simplest extensions of the SM scalar sector is the so-called 2HDM [7], in which a second scalar doublet

is added to the SM field content. The added scalar doublet can provide additional sources of CP violation besides that from the Cabibbo-Kobayashi-Maskawa (CKM) [8, 9] matrix, making it possible to explain the BAU [4].

It is known that, within the SM, the flavor-changing neutral current (FCNC) interactions are forbidden at tree level and are also highly suppressed at higher orders, due to the Glashow-Iliopoulos-Maiani mechanism [10]. To avoid the experimental constraints on the FCNCs, the natural flavor conservation (NFC) [11] and minimal flavor violation (MFV) [12–15] hypotheses have been proposed (the NFC and MFV hypotheses are not the only alternatives to avoid constraints from FCNCs; models with controlled FCNCs have also been addressed in the literature [16–20]). In the NFC hypothesis, the absence of dangerous FCNCs is guaranteed by limiting the number of scalar doublets coupling to a given type of right-handed fermion to be at most one. This can be explicitly achieved by applying a discrete \mathcal{Z}_2 symmetry to the two scalar doublets differently, leading to four types of 2HDM

(usually named as types I, II, X, and Y) [21, 22], which have been studied extensively for many years. In the MFV hypothesis, to control the flavor-violating interactions, all the scalar Yukawa couplings are assumed to be composed of the SM ones Y^U and Y^D . In the ‘‘Higgs basis’’ [23], in which only one doublet gets a nonzero vacuum expectation value (VEV) and behaves the same as the SM one, the allowed $SU(3) \times SU(2) \times U(1)$ representation of the second scalar doublet is fixed to be either $(1, 2)_{1/2}$ or $(8, 2)_{1/2}$ [24], which implies that the second scalar doublet can be either color-singlet or color-octet. For convenience, they are referred as type III and type C model [25], respectively. Examples of the color-singlet case include the aligned 2HDM (A2HDM) [26, 27] and the four types of 2HDM reviewed in [21, 22]. In the color-octet case, the scalar spectrum contains one CP-even, color-singlet Higgs boson (the usual SM one), and three color-octet particles, one CP-even, one CP-odd, and one electrically charged [24].

Although the scalar-mediated flavor-violating interactions are protected by the MFV hypothesis, type III and type C models can still bring in many interesting phenomena in some low-energy processes, especially due to the presence of a charged-Higgs boson [24, 25, 28–32]. The neutral-meson mixings are of particular interest in this respect, because the charged-Higgs contributions to these processes arise at the same order as does the W boson in the SM, indicating that the NP effects might be significant. For example, the charged-Higgs effects of these two models on the $B_s^0 - \bar{B}_s^0$ mixing have been studied in [28]. In this paper, we shall explore the $K^0 - \bar{K}^0$ mixing within these two models and pursue possible differences between their effects. The general formula for $K^0 - \bar{K}^0$ mixing, including the charged-Higgs contributions, could be found, for example, in [33].

Our paper is organized as follows. In Section 2, we review briefly the 2HDMs under the MFV hypothesis and give the theoretical framework for the $K^0 - \bar{K}^0$ mixing. In Section 3, we perform a complete one-loop computation of the Wilson coefficients for the process within these two models. In Section 4, numerical results and discussions are presented in detail. Finally, our conclusions are made in Section 5. Explicit expressions for the loop functions appearing in the $K^0 - \bar{K}^0$ mixing are collected in the appendix.

2. Theoretical Framework

2.1. Yukawa Sector. Specifying to the ‘‘Higgs basis’’ [23], in which only one doublet gets a nonzero VEV, we can write the most general Lagrangian of Yukawa couplings between the two Higgs doublets, Φ_1 and Φ_2 , and quarks as [24, 25]

$$-\mathcal{L}_Y = \bar{q}_L^0 \tilde{\Phi}_1 Y^U u_R^0 + \bar{q}_L^0 \Phi_1 Y^D d_R^0 + \bar{q}_L^0 \tilde{\Phi}_2^{(a)} T_R^{(a)} \bar{Y}^U u_R^0 + \bar{q}_L^0 \Phi_2^{(a)} T_R^{(a)} \bar{Y}^D d_R^0 + \text{h.c.}, \quad (1)$$

where $\tilde{\Phi}_j = i\sigma_2 \Phi_j^*$ ($j = 1, 2$) with σ_2 the Pauli matrix, and \bar{q}_L^0 , u_R^0 , and d_R^0 are the quark fields given in the interaction basis. $T_R^{(a)}$ is the $SU(3)$ color generator which determines the color

nature of the second Higgs doublet (depending on which type of 2HDM we are considering, the second Higgs doublet can be either color-singlet or color-octet). $Y^{U,D}$ and $\bar{Y}^{U,D}$ are the Yukawa couplings and are generally complex 3×3 matrices in the quark flavor space.

According to the MFV hypothesis, the transformation properties of the Yukawa coupling matrices $Y^{U,D}$ and $\bar{Y}^{U,D}$ under the quark flavor symmetry group $SU(3)_{Q_L} \otimes SU(3)_{U_R} \otimes SU(3)_{D_R}$ are required to be the same. This can be achieved by requiring $\bar{Y}^{U,D}$ to be composed of pairs of $Y^{U,D}$ [25]:

$$\begin{aligned} \bar{Y}^U &= A_u^* (1 + \epsilon_u^* Y^U Y^{U\dagger} + \dots) Y^U, \\ \bar{Y}^D &= A_d (1 + \epsilon_d Y^D Y^{D\dagger} + \dots) Y^D. \end{aligned} \quad (2)$$

Transforming the Lagrangian in (1) from the interaction basis to the mass basis, one can obtain the Yukawa interactions of charged Higgs with quarks in the mass-eigenstate basis, which are given by [25, 28]

$$\begin{aligned} \mathcal{L}_{H^\pm} &= \frac{g}{\sqrt{2}m_W} \sum_{i,j=1}^3 \bar{u}_i T_R^{(a)} (A_u^i m_{u_i} P_L - A_d^i m_{d_j} P_R) V_{ij} d_j H_{(a)}^\pm \\ &+ \text{h.c.}, \end{aligned} \quad (3)$$

where $A_{u,d}^i$ are family-dependent Yukawa coupling constants [25, 28, 34]:

$$A_{u,d}^i = A_{u,d} \left(1 + \epsilon_{u,d} \frac{m_t^2}{v^2} \delta_{i3} \right), \quad (4)$$

with $v = \langle \Phi_1^0 \rangle = 174$ GeV. For simplicity, we consider only the family universal coupling case in which the family-dependent Yukawa couplings, $A_{u,d}^i$, can be simplified to $A_{u,d}^i = A_{u,d}$.

2.2. $K^0 - \bar{K}^0$ Mixing. Both within the SM and in the 2HDMs with MFV, the neutral kaon mixing occurs via the box diagrams depicted in Figure 1 (these Feynman diagrams are drawn with the LaTeX package *TikZ-Feynman* [35]). As demonstrated in [36], the correction from the external momenta and quark masses is not negligible for the $K^0 - \bar{K}^0$ mixing. Thus, unlike the traditional calculation performed in the limit of vanishing external momenta and external quark masses, we shall keep the external strange-quark momentum and mass to the second order; this is essential to guarantee the final result gauge-independent [34].

Calculating the one-loop box diagrams and following the standard procedure of matching [36], we obtain the effective Hamiltonian responsible for the $K^0 - \bar{K}^0$ mixing:

$$\begin{aligned} \mathcal{H}_{\text{eff}} &= \frac{G_F^2 m_W^2}{16\pi^2} [C^{\text{VLL}}(\mu) Q^{\text{VLL}} + C^{\text{SLL}}(\mu) Q^{\text{SLL}} \\ &+ C^{\text{TLL}}(\mu) Q^{\text{TLL}}] + \text{h.c.}, \end{aligned} \quad (5)$$

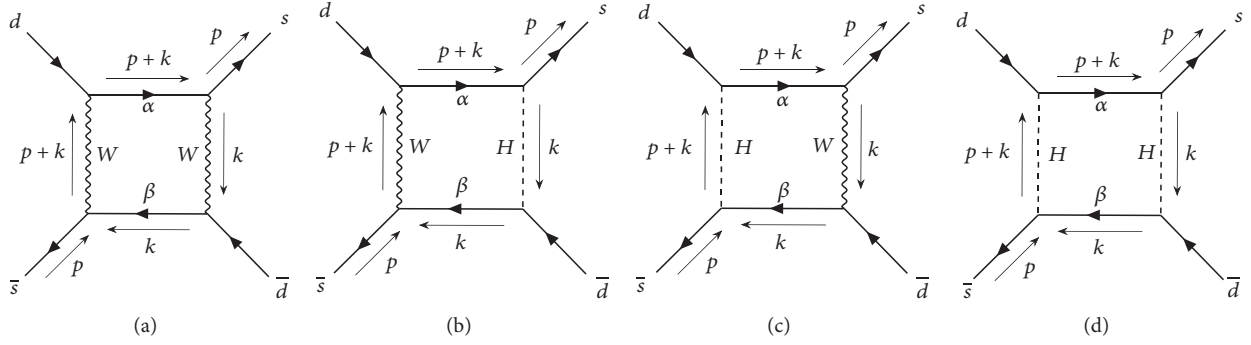


FIGURE 1: Box diagrams for the $K^0 - \bar{K}^0$ mixing in the unitary gauge both within the SM (a) and in the 2HDMs with MFV (b)–(d). Crossed diagrams, which are related to the original ones by interchanging the external lines, have also been taken into account.

where G_F is the Fermi coupling constant, m_W is the W -boson mass, and $C_i(\mu)$ is the scale-dependent Wilson coefficients of the four-quark operators Q_i , which are defined, respectively, as follows (there are totally eight four-quark operators for the most general case [37], but we have written out only the operators that exist in our calculation):

$$\begin{aligned} Q^{\text{VLL}} &= \bar{s}^\alpha \gamma_\mu (1 - \gamma_5) d^\alpha \bar{s}^\beta \gamma^\mu (1 - \gamma_5) d^\beta, \\ Q^{\text{SLL}} &= \bar{s}^\alpha (1 - \gamma_5) d^\alpha \bar{s}^\beta (1 - \gamma_5) d^\beta, \\ Q^{\text{TLL}} &= \bar{s}^\alpha \sigma_{\mu\nu} (1 - \gamma_5) d^\alpha \bar{s}^\beta \sigma^{\mu\nu} (1 - \gamma_5) d^\beta, \end{aligned} \quad (6)$$

with α and β being the color indices and $\sigma_{\mu\nu} = (1/2)[\gamma_\mu, \gamma_\nu]$. Note that we include the QCD corrections only to the SM Wilson coefficient C^{VLL} , but not to the NP ones. The hadronic matrix elements of these operators can be written as [37]

$$\begin{aligned} \langle \bar{K}^0 | Q^{\text{VLL}} | K^0 \rangle &= \frac{4}{3} m_K F_K^2 B_1^{\text{VLL}}(\mu), \\ \langle \bar{K}^0 | Q^{\text{SLL}} | K^0 \rangle &= -\frac{5}{6} R(\mu) m_K F_K^2 B_1^{\text{SLL}}(\mu), \\ \langle \bar{K}^0 | Q^{\text{TLL}} | K^0 \rangle &= -2R(\mu) m_K F_K^2 B_2^{\text{SLL}}(\mu), \end{aligned} \quad (7)$$

where m_K is the kaon mass and F_K the kaon decay constant. $B_i^j(\mu)$ is the scale-dependent bag parameters, and $R(\mu)$ is defined as [37]

$$R(\mu) = \left(\frac{m_K}{m_s(\mu) + m_d(\mu)} \right)^2. \quad (8)$$

It should be noted that the SM and NP contributions to the Wilson coefficients $C^i(\mu)$ cannot be summed directly because they are given at different initial scales, μ_W for the SM and μ_{H^\pm} for the 2HDM in particular. In order to sum these two contributions, they must be firstly run down to the lattice scale at which the bag parameters $B_i^j(\mu)$ are evaluated. The explicit expressions for these Wilson coefficients will be presented in Section 3.

For the $K^0 - \bar{K}^0$ mixing, there exist two observables which can be calculated from the effective Hamiltonian given by (5) [37]:

$$\Delta m_K = 2\text{Re} \langle K^0 | \mathcal{H}_{\text{eff}} | \bar{K}^0 \rangle, \quad (9)$$

$$\epsilon_K = \frac{\exp(i\pi/4)}{\sqrt{2}\Delta m_K} \text{Im} \langle K^0 | \mathcal{H}_{\text{eff}} | \bar{K}^0 \rangle. \quad (10)$$

The above equations are the most general formulae for these two observables. It should be noted that Δm_K and ϵ_K receive both short-distance (SD) and long-distance (LD) contributions. With the LD contribution included, the mass difference Δm_K can be decomposed as [38]

$$\Delta m_K = \Delta m_K^{\text{SD}} + \Delta m_K^{\text{LD}}|_{\pi\pi} + \Delta m_K^{\text{LD}}|_{\eta'}. \quad (11)$$

where the SD part is derived from (9) with the effective Hamiltonian obtained from the box diagrams, while the two LD parts are estimated, respectively, as [38, 39]

$$\begin{aligned} \Delta m_K^{\text{LD}}|_{\pi\pi} &= 0.4\Delta m_K^{\text{exp}}, \\ \Delta m_K^{\text{LD}}|_{\eta'} &= -0.3\Delta m_K^{\text{exp}}. \end{aligned} \quad (12)$$

We can see from (12) that the LD contribution to Δm_K is about 10% of the experimental value. However, keeping in mind that this estimate is just a bold-guess based on an analysis at the leading chiral logarithm in the framework of chiral perturbation theory [38], we should note that the actual uncertainty on Δm_K^{LD} is quite huge (we thank Professor Antonio Pich for pointing out this to us). As the structure of LD contribution is still not well understood, we include this part only in the SM case but not in the NP one.

The formula for the CP-violating parameter ϵ_K , with the LD contribution taken into account, is given by [40]

$$\epsilon_K = \frac{\kappa_\epsilon e^{i\phi_\epsilon}}{\sqrt{2}} \frac{\text{Im} M_{12}^{\text{SD}}}{\Delta m_K^{\text{exp}}}, \quad (13)$$

where $\kappa_\epsilon = 0.94(2)$ [38], $\phi_\epsilon = 43.52(5)^\circ$ [41], and $M_{12}^{\text{SD}} = \langle K^0 | \mathcal{H}_{\text{eff}} | \bar{K}^0 \rangle$. The LD contribution to ϵ_K has been included in

the two phenomenological factors κ_ϵ and ϕ_ϵ . In the case with only the SD contribution, $\kappa_\epsilon = 1$ and $\phi_\epsilon = \pi/4$, and (13) goes back to (10).

3. Analytic Calculation

3.1. Wilson Coefficients within the SM. For the SM case, we calculate the Wilson coefficients from the box diagram shown in Figure 1(a). Without any QCD correction, they are given, respectively, as

$$\begin{aligned}
C_{SM}^{VLL}(\mu_W) &= [\lambda_c^2 S_0(x_c) + \lambda_t^2 S_0(x_t) + 2\lambda_c \lambda_t S_0(x_c, x_t)] \\
&\quad + x_s [\lambda_c^2 f_1(x_c) + \lambda_t^2 f_1(x_t) + 2\lambda_c \lambda_t f_1(x_c, x_t)], \\
C_{SM}^{SLL}(\mu_W) &= x_s [\lambda_c^2 f_2(x_c) + \lambda_t^2 f_2(x_t) + 2\lambda_c \lambda_t f_2(x_c, x_t)], \\
C_{SM}^{TLL}(\mu_W) &= x_s [\lambda_c^2 f_3(x_c) + \lambda_t^2 f_3(x_t) + 2\lambda_c \lambda_t f_3(x_c, x_t)],
\end{aligned} \tag{14}$$

where $x_i = m_i^2(\mu)/m_W^2$, and S_0 is the Inami-Lim function given by (A.1) [42]. Explicit expressions for the functions f_i can be found in the appendix. Note that when the external strange-quark momentum and mass are kept to the second order, we also get nonzero contributions to the Wilson coefficients C_{SM}^{SLL} and C_{SM}^{TLL} even in the SM case.

The QCD corrections to the Wilson coefficients can be described by the factors η_{cc} , η_{ct} , and η_{tt} , which have been calculated up to the next-to-next-to-leading order [43–45] and are collected in [46]. Combining the renormalization group (RG) evolution with these QCD corrections, we get

$$\begin{aligned}
\langle \bar{K}^0 | \mathcal{H}_{\text{eff}} | K^0 \rangle_{SM}^{VLL} &= \zeta [\hat{B}(\lambda_c^2 \eta_{cc} S_0(\bar{x}_c) \\
&\quad + \lambda_t^2 \eta_{tt} S_0(\bar{x}_t) + 2\lambda_c \lambda_t \eta_{ct} S_0(\bar{x}_c, \bar{x}_t)) \\
&\quad + P_{SM}^{VLL} x_{s, \mu_W} (\lambda_c^2 f_1(x_{c, \mu_W}) + \lambda_t^2 f_1(x_{t, \mu_W}) \\
&\quad + 2\lambda_c \lambda_t f_1(x_{c, \mu_W}, x_{t, \mu_W}))], \\
\langle \bar{K}^0 | \mathcal{H}_{\text{eff}} | K^0 \rangle_{SM}^{SLL} &= \zeta [P_{SM}^{SLL} C_{SM}^{SLL}(\mu_W)], \\
\langle \bar{K}^0 | \mathcal{H}_{\text{eff}} | K^0 \rangle_{SM}^{TLL} &= \zeta [P_{SM}^{TLL} C_{SM}^{TLL}(\mu_W)],
\end{aligned} \tag{15}$$

where $\zeta = G_F^2 m_K^2 m_K F_K^2 / 12\pi^2$, and $\bar{x}_i \equiv (m_i(m_i)/m_W)^2$ is the scale-independent mass ratio, whereas $x_{i, \mu} \equiv (m_i(\mu)/m_W)^2$ is the mass ratio at the scale μ . \hat{B} is the RG independent bag

parameter, and the factors P^j encode the RG evolution effects that are given, respectively, as [37]

$$\begin{aligned}
P_{SM}^{VLL} &= [\eta(3 \text{ GeV})]_{VLL}^{SM} B_1(3 \text{ GeV}), \\
P_{SM}^{SLL} &= -\frac{5}{8} [\eta_{11}(3 \text{ GeV})]_{SLL}^{SM} [B_2(3 \text{ GeV})]_{\text{eff}} \\
&\quad - \frac{3}{2} [\eta_{21}(3 \text{ GeV})]_{SLL}^{SM} [B_3(3 \text{ GeV})]_{\text{eff}}, \\
P_{SM}^{TLL} &= -\frac{5}{8} [\eta_{12}(3 \text{ GeV})]_{SLL}^{SM} [B_2(3 \text{ GeV})]_{\text{eff}} \\
&\quad - \frac{3}{2} [\eta_{22}(3 \text{ GeV})]_{SLL}^{SM} [B_3(3 \text{ GeV})]_{\text{eff}},
\end{aligned} \tag{16}$$

where the effective bag parameters $[B_i(3 \text{ GeV})]_{\text{eff}}$ are defined as [37]

$$[B_i(3 \text{ GeV})]_{\text{eff}} \equiv R(3 \text{ GeV}) B_i(3 \text{ GeV}), \tag{17}$$

with $R(\mu)$ defined in (8). The factors η and $\eta_{i,j}$ are given by the formulae collected in [37] with

$$\begin{aligned}
\eta_4 &\equiv \frac{\alpha_s^{(4)}(\mu_b)}{\alpha_s^{(4)}(3 \text{ GeV})}, \\
\eta_5 &\equiv \frac{\alpha_s^{(5)}(\mu_W)}{\alpha_s^{(5)}(\mu_b)}.
\end{aligned} \tag{18}$$

3.2. Wilson Coefficients in the 2HDMs with MFV. The Wilson coefficients at the matching scale $\mu_{H^\pm} \sim m_{H^\pm}$ in the NP case are calculated from the box diagrams shown in Figures 1(b)–1(d), with the results given, respectively, as

$$\begin{aligned}
C_{III}^{VLL}(\mu_{H^\pm}) &= A_u A_u^* [\lambda_c^2 (f_4(x_c, x_H) \\
&\quad + x_s g_4(x_c, x_H)) + \lambda_t^2 (f_4(x_t, x_H) + x_s g_4(x_t, x_H)) \\
&\quad + 2\lambda_c \lambda_t (f_4(x_c, x_t, x_H) + x_s g_4(x_c, x_t, x_H))] \\
&\quad + A_u A_d^* x_s [\lambda_c^2 f_5(x_c, x_H) + \lambda_t^2 f_5(x_t, x_H) \\
&\quad + 2\lambda_c \lambda_t f_5(x_c, x_t, x_H)] + A_u^2 A_u^{*2} x_s [\lambda_c^2 f_6(x_c, x_H) \\
&\quad + \lambda_t^2 f_6(x_t, x_H) + 2\lambda_c \lambda_t f_6(x_c, x_t, x_H)], \\
C_{III}^{SLL}(\mu_{H^\pm}) &= x_s [A_u A_u^* (\lambda_c^2 [f_7(x_c, x_H) + g_7(x_c, x_H)] \\
&\quad + \lambda_t^2 [f_7(x_t, x_H) + g_7(x_t, x_H)])
\end{aligned}$$

$$\begin{aligned}
& + 2\lambda_c \lambda_t [f_7(x_c, x_t, x_H) + g_7(x_c, x_t, x_H)] \\
& + A_u A_d^* (\lambda_c^2 f_8(x_c, x_H) + \lambda_t^2 f_8(x_t, x_H) \\
& + 2\lambda_c \lambda_t f_8(x_c, x_t, x_H)) + A_u^2 A_u^{*2} (\lambda_c^2 f_9(x_c, x_H) \\
& + \lambda_t^2 f_9(x_t, x_H) + 2\lambda_c \lambda_t f_9(x_c, x_t, x_H)) \\
& + A_u^2 A_d^{*2} (\lambda_c^2 f_{10}(x_c, x_H) + \lambda_t^2 f_{10}(x_t, x_H) \\
& + 2\lambda_c \lambda_t f_{10}(x_c, x_t, x_H)) \\
& - A_u^2 A_u^* A_d^* (\lambda_c^2 f_{10}(x_c, x_H) + \lambda_t^2 f_{10}(x_t, x_H) \\
& + 2\lambda_c \lambda_t f_{10}(x_c, x_t, x_H))] , \\
C_{\text{III}}^{\text{TLL}}(\mu_{H^\pm}) &= 0, \\
C_{\text{C}}^{\text{VLL}}(\mu_{H^\pm}) &= \frac{1}{3} A_u A_u^* [\lambda_c^2 (f_4(x_c, x_H) \\
& + x_s g_4(x_c, x_H)) + \lambda_t^2 (f_4(x_t, x_H) + x_s g_4(x_t, x_H)) \\
& + 2\lambda_c \lambda_t (f_4(x_c, x_t, x_H) + x_s g_4(x_c, x_t, x_H))] + \frac{1}{3} \\
& \cdot A_u A_d^* x_s [\lambda_c^2 f_5(x_c, x_H) + \lambda_t^2 f_5(x_t, x_H) \\
& + 2\lambda_c \lambda_t f_5(x_c, x_t, x_H)] + \frac{11}{18} \\
& \cdot A_u^2 A_u^{*2} x_s [\lambda_c^2 f_6(x_c, x_H) + \lambda_t^2 f_6(x_t, x_H) \\
& + 2\lambda_c \lambda_t f_6(x_c, x_t, x_H)] , \\
C_{\text{C}}^{\text{SLL}}(\mu_{H^\pm}) &= x_s \left[-\frac{5}{12} \right. \\
& \cdot A_u A_u^* (\lambda_c^2 [f_7(x_c, x_H) + g_7(x_c, x_H)] \\
& + \lambda_t^2 [f_7(x_t, x_H) + g_7(x_t, x_H)] \\
& + 2\lambda_c \lambda_t [f_7(x_c, x_t, x_H) + g_7(x_c, x_t, x_H)]) - \frac{5}{12} \\
& \cdot A_u A_d^* (\lambda_c^2 f_8(x_c, x_H) + \lambda_t^2 f_8(x_t, x_H) \\
& + 2\lambda_c \lambda_t f_8(x_c, x_t, x_H)) - \frac{19}{72} \\
& \cdot A_u^2 A_u^{*2} (\lambda_c^2 f_9(x_c, x_H) + \lambda_t^2 f_9(x_t, x_H) \\
& + 2\lambda_c \lambda_t f_9(x_c, x_t, x_H)) - \frac{19}{72} \\
& \cdot A_u^2 A_d^{*2} (\lambda_c^2 f_{10}(x_c, x_H) + \lambda_t^2 f_{10}(x_t, x_H) \\
& + 2\lambda_c \lambda_t f_{10}(x_c, x_t, x_H)) + \frac{19}{72} \\
& \left. \cdot A_u^2 A_u^* A_d^* (\lambda_c^2 f_{10}(x_c, x_H) + \lambda_t^2 f_{10}(x_t, x_H) \right. \\
& \left. + 2\lambda_c \lambda_t f_{10}(x_c, x_t, x_H)) \right] ,
\end{aligned}$$

$$\begin{aligned}
C_{\text{C}}^{\text{TLL}}(\mu_{H^\pm}) &= x_s \left[\frac{1}{16} \right. \\
& \cdot A_u A_u^* (\lambda_c^2 [f_7(x_c, x_H) + g_7(x_c, x_H)] \\
& + \lambda_t^2 [f_7(x_t, x_H) + g_7(x_t, x_H)] \\
& + 2\lambda_c \lambda_t [f_7(x_c, x_t, x_H) + g_7(x_c, x_t, x_H)]) + \frac{1}{16} \\
& \cdot A_u A_d^* (\lambda_c^2 f_8(x_c, x_H) + \lambda_t^2 f_8(x_t, x_H) \\
& + 2\lambda_c \lambda_t f_8(x_c, x_t, x_H)) + \frac{7}{96} \\
& \cdot A_u^2 A_u^{*2} (\lambda_c^2 f_9(x_c, x_H) + \lambda_t^2 f_9(x_t, x_H) \\
& + 2\lambda_c \lambda_t f_9(x_c, x_t, x_H)) + \frac{7}{96} \\
& \cdot A_u^2 A_d^{*2} (\lambda_c^2 f_{10}(x_c, x_H) + \lambda_t^2 f_{10}(x_t, x_H) \\
& + 2\lambda_c \lambda_t f_{10}(x_c, x_t, x_H)) - \frac{7}{96} \\
& \left. \cdot A_u^2 A_u^* A_d^* (\lambda_c^2 f_{10}(x_c, x_H) + \lambda_t^2 f_{10}(x_t, x_H) \right. \\
& \left. + 2\lambda_c \lambda_t f_{10}(x_c, x_t, x_H)) \right] . \tag{19}
\end{aligned}$$

Explicit expressions for the functions f_i introduced in the above equations are collected in the appendix. Note that the contribution to $C_{\text{III}}^{\text{TLL}}$ is zero for type III but is not for type C 2HDM. With the RG evolution effect included, the final result is similar to the SM case and can be written as

$$\begin{aligned}
\langle \bar{K}^0 | \mathcal{H}_{\text{eff}} | K^0 \rangle_{\text{III}}^{\text{VLL}} &= \zeta [P_{\text{NP}}^{\text{VLL}} C_{\text{III}}^{\text{VLL}}(\mu_t)] , \\
\langle \bar{K}^0 | \mathcal{H}_{\text{eff}} | K^0 \rangle_{\text{III}}^{\text{SLL}} &= \zeta [P_{\text{NP}}^{\text{SLL}} C_{\text{III}}^{\text{SLL}}(\mu_t)] , \tag{20} \\
\langle \bar{K}^0 | \mathcal{H}_{\text{eff}} | K^0 \rangle_{\text{III}}^{\text{TLL}} &= 0,
\end{aligned}$$

for type III, and

$$\begin{aligned}
\langle \bar{K}^0 | \mathcal{H}_{\text{eff}} | K^0 \rangle_{\text{C}}^{\text{VLL}} &= \zeta [P_{\text{NP}}^{\text{VLL}} C_{\text{C}}^{\text{VLL}}(\mu_t)] , \\
\langle \bar{K}^0 | \mathcal{H}_{\text{eff}} | K^0 \rangle_{\text{C}}^{\text{SLL}} &= \zeta [P_{\text{NP}}^{\text{SLL}} C_{\text{C}}^{\text{SLL}}(\mu_t)] , \tag{21} \\
\langle \bar{K}^0 | \mathcal{H}_{\text{eff}} | K^0 \rangle_{\text{C}}^{\text{TLL}} &= \zeta [P_{\text{NP}}^{\text{TLL}} C_{\text{C}}^{\text{TLL}}(\mu_t)] ,
\end{aligned}$$

for type C 2HDM. The factors P^i are also similar to the SM case but with a different factor η_5 , which is now defined by

$$\eta_5 \equiv \frac{\alpha_s^{(5)}(\mu_t)}{\alpha_s^{(5)}(\mu_b)} . \tag{22}$$

Here the matching scale for the 2HDMs has been changed to $\mu_t \sim m_t$, because the evolution effect from $\mu_{H^\pm} \sim m_{H^\pm}$ down to $\mu_t \sim m_t$ is quite small and can be safely neglected.

TABLE 1: Input parameters used throughout this paper, together with the experimental data.

Electroweak parameters [47]	
$m_W = 80.385(15)$ GeV	$m_Z = 91.1876(21)$ GeV
$\mu_W = 80.385$ GeV	$\mu_t = 163.427$ GeV ^a
$G_F = 1.1663787(6) \times 10^{-5}$ GeV ⁻²	
QCD coupling constant	
$\alpha_s(\mu_t) = 0.1086(10)^a$	$\alpha_s(m_Z) = 0.1182(12)$ [47]
$\alpha_s(\mu_W) = 0.1205(12)^a$	$\alpha_s(\mu_b) = 0.2243(45)^a$
$\alpha_s(3 \text{ GeV}) = 0.2521^{+0.0058^a}_{-0.0057}$	
Quark masses	
$m_d(2 \text{ GeV}) = 0.0047^{+0.0005}_{-0.0004}$ GeV [47]	$m_d(3 \text{ GeV}) = 0.0043^{+0.0005}_{-0.0004}$ GeV ^a
$m_s(2 \text{ GeV}) = 0.096^{+0.008}_{-0.004}$ GeV [47]	$m_s(3 \text{ GeV}) = 0.087^{+0.007}_{-0.004}$ GeV ^a
$m_s(\mu_W) = 0.057^{+0.005}_{-0.002}$ GeV ^a	$m_s(\mu_t) = 0.054^{+0.005}_{-0.002}$ GeV ^a
$m_c(m_c) = 1.27(3)$ GeV [47]	$m_c(\mu_W) = 0.660(21)$ GeV ^a
$m_c(\mu_t) = 0.623(20)$ GeV ^a	$m_t^{\text{pole}} = 173.21(87)$ GeV [47]
$m_t(m_t) = 163.427^{+0.828}_{-0.829}$ GeV ^a	$m_t(\mu_W) = 173.276^{+1.590}_{-1.586}$ GeV ^a
CKM matrix elements [47]	
$\lambda = 0.22506(50)$	$A = 0.811(26)$
$\bar{\rho} = 0.124^{+0.019}_{-0.018}$	$\bar{\eta} = 0.356(11)$
$\rho = 0.127^{+0.019}_{-0.018}$	$\eta = 0.365(11)$
Kaon mixing parameters	
$m_K = 0.497611(13)$ GeV [47]	$F_K = 0.1562(9)$ GeV [41]
$\hat{B}_K = 0.7625(97)$ [41]	$B_1(3 \text{ GeV}) = 0.519(26)$ [48]
$B_2(3 \text{ GeV}) = 0.525(23)$ [48]	$B_3(3 \text{ GeV}) = 0.360(16)$ [48]
$B_4(3 \text{ GeV}) = 0.981(62)$ [48]	$B_5(3 \text{ GeV}) = 0.751(68)$ [48]
$\eta_{cc} = 1.87(76)$ [46]	$\eta_{tt} = 0.5765(65)$ [46]
$\eta_{ct} = 0.496(47)$ [46]	
Experimental data [47]	
$(\Delta m_K)_{\text{exp}} = 3.4839(59) \times 10^{-15}$ GeV	$(\epsilon_K)_{\text{exp}} = 2.228(11) \times 10^{-3}$

^aThis value is calculated with the *RunDec* package [49] at the two-loop level in α_s .

After performing the proper RG evolution, we can then sum directly both the SM and NP contributions to the matrix element $\langle \bar{K}^0 | \mathcal{H}_{\text{eff}} | K^0 \rangle$, which can be written as

$$\begin{aligned} \langle \bar{K}^0 | \mathcal{H}_{\text{eff}} | K^0 \rangle^i &= \langle \bar{K}^0 | \mathcal{H}_{\text{eff}} | K^0 \rangle_{\text{SM}}^i \\ &+ \langle \bar{K}^0 | \mathcal{H}_{\text{eff}} | K^0 \rangle_{\text{NP}}^i, \end{aligned} \quad (23)$$

where the superscript “*i*” labels the different four-quark operators.

4. Numerical Results and Discussions

4.1. Input Parameters and the SM Results. Firstly, we collect in Table 1 the values of the relevant input parameters used throughout this paper, together with the experimental data on Δm_K and ϵ_K . For the bag parameters, we use the lattice results with $N_f = 2 + 1$ flavors of dynamical quarks and evaluated at the renormalization scale 3 GeV [41, 48]. In addition, we have used the *RunDec* package [49] to obtain the running coupling

constant and quark masses at different scales in the two-loop approximation.

With the input parameters collected in Table 1, we can now give the numerical results for Δm_K and ϵ_K in the SM case, which are listed in Table 2. We make the following comments on the SM results:

- (i) Our result for the mass difference Δm_K without the corrections from the external strange-quark mass, x_s , and from the LD contribution, agrees well with that obtained in [45].
- (ii) The corrections from x_s to Δm_K and ϵ_K are 6.83% and -0.06% , respectively. Note that the correction to Δm_K is at the same order as that obtained in [36]. Moreover, the LD contributions to Δm_K and ϵ_K are 11.20% and -6% , respectively.
- (iii) As the x_s correction can be precisely calculated, we consider it both to Δm_K and to ϵ_K ; especially, this correction is not too small for Δm_K . In addition, we include the LD contributions to ϵ_K but not to Δm_K , because the structure of LD contribution to Δm_K is still not well understood [38].

TABLE 2: SM results for Δm_K and ϵ_K with different corrections included and the ratios between these values and their experimental data. Here the column “None” denotes the results obtained with the external strange-quark momentum and mass ignored and without including the LD contribution.

Observables	Corrections			
	None	With LD	With x_s	With LD and x_s
$(\Delta m_K)_{\text{SM}} (\times 10^{-15} \text{ GeV})$	3.109 (1.258)	3.458 (1.258)	3.321 (1.258)	3.670 (1.258)
$\frac{(\Delta m_K)_{\text{SM}}}{(\Delta m_K)_{\text{exp}}}$	89.24%	99.24%	95.34%	105.34%
$(\epsilon_K)_{\text{SM}} (\times 10^{-3})$	$2.219^{+0.309}_{-0.294}$	$2.086^{+0.294}_{-0.280}$	$2.218^{+0.309}_{-0.294}$	$2.085^{+0.294}_{-0.280}$
$\frac{(\epsilon_K)_{\text{SM}}}{(\epsilon_K)_{\text{exp}}}$	99.61%	93.63%	99.55%	93.58%

4.2. *Results in the 2HDMs with MFV.* As can be seen clearly from Table 2, there is no significant deviation between the SM predictions and the experimental data for Δm_K and ϵ_K , especially for the latter. Therefore, these two observables are expected to put strong constraints on the parameter spaces of type III and type C 2HDMs, which are both featured by the three parameters, the two Yukawa couplings $A_{u,d}$, and the charged-Higgs mass m_{H^\pm} , in this paper. In the case of complex couplings, we can further choose $|A_u|$ and $A_u A_d^* = |A_u A_d^*| e^{i\theta}$ as the independent variables, with θ being the relative phase between A_u and A_d^* .

The relevant model parameters are also constrained by the other processes. For the parameter $|A_u|$, an upper bound can be obtained from the $Z \rightarrow b\bar{b}$ decay [25], while the parameter A_d is much less constrained phenomenologically [25, 28]. However, the perturbativity of the theory requires that these couplings cannot be too large. As for the charged-Higgs mass, the lower bound $m_{H^\pm} > 78.6 \text{ GeV}$ (95% CL) has been set by the LEP experiment [50], which is obtained under the assumption that H^\pm decays mainly into fermions without any specific Yukawa structure. In addition, direct searches for H^\pm are also performed by the Tevatron [51], ATLAS [52], and CMS [53] experiments, among which most constraints depend strongly on the underlying Yukawa structures. Recently, by comparing the cross-sections for the dijet, top-pair, dijet-pair, $t\bar{t}b\bar{t}$, and $b\bar{b}b\bar{b}$ production at the LHC with the strongest available experimental limits from ATLAS or CMS at 8 or 13 TeV, Hayreter, and Valencia [54] has extracted constraints on the parameter space of the Manohar-Wise model [24], which is equivalent to type C 2HDM discussed here. Interestingly, they found that masses below 1 TeV have not been excluded for color-octet scalars as is often claimed in the literature. For a variety of well-motivated 2HDMs, the authors in [55] found that charged-Higgs bosons as light as 75 GeV can still be compatible with all the results from direct charged and neutral Higgs boson searches at LEP and the LHC, as well as the most recent constraints from flavor physics, although this implies severely suppressed charged-Higgs couplings to all fermions. Thus, based on the above observations, we generate randomly numerical points for the model parameters as [34]

$$\begin{aligned} |A_u| &\in [0, 3], \\ |A_d| &\in [0, 500], \end{aligned}$$

$$\theta \in [-\pi, \pi],$$

$$m_{H^\pm} = 100, 250, 500 \text{ GeV.}$$

(24)

Taking $m_{H^\pm} = 500 \text{ GeV}$ as a benchmark, we firstly explore the dependence of each Wilson coefficient evaluated at the matching scale $\mu = m_{H^\pm}$ or approximately at $\mu = m_t$ on the other model parameters,

$$\begin{aligned} C_{\text{III}}^{\text{VLL}} \times 10^9 &= (41.28 - 42.15i) |A_u|^2 \\ &\quad + (6.97 - 7.19i) |A_u|^4 + 10^{-4} \\ &\quad \cdot (5.33 - 0.05i) A_u A_d^*, \\ C_{\text{III}}^{\text{SLL}} \times 10^{15} &= (3.28 - 3.29i) |A_u|^2 \\ &\quad - (0.09 - 0.09i) |A_u|^4 \\ &\quad - (308.73 - 25.25i) A_u A_d^* \\ &\quad + (0.45 - 0.46i) |A_u|^2 A_u A_d^* \\ &\quad - (0.45 - 0.46i) (A_u A_d^*)^2, \\ C_{\text{C}}^{\text{VLL}} \times 10^9 &= (13.76 - 14.05i) |A_u|^2 \\ &\quad + (4.26 - 4.39i) |A_u|^4 + 10^{-4} \\ &\quad \cdot (1.78 - 0.02i) A_u A_d^*, \\ C_{\text{C}}^{\text{SLL}} \times 10^{15} &= -(1.37 - 1.37i) |A_u|^2 \\ &\quad + (0.02 - 0.02i) |A_u|^4 \\ &\quad + (128.64 - 10.52i) A_u A_d^* \\ &\quad - (0.12 - 0.12i) |A_u|^2 A_u A_d^* \\ &\quad + (0.12 - 0.12i) (A_u A_d^*)^2, \\ C_{\text{C}}^{\text{TLL}} \times 10^{16} &= (2.05 - 2.06i) |A_u|^2 \\ &\quad - (0.06 - 0.06i) |A_u|^4 \\ &\quad - (192.96 - 15.78i) A_u A_d^* \\ &\quad + (0.32 - 0.33i) |A_u|^2 A_u A_d^* \\ &\quad - (0.32 - 0.33i) (A_u A_d^*)^2. \end{aligned} \tag{25}$$

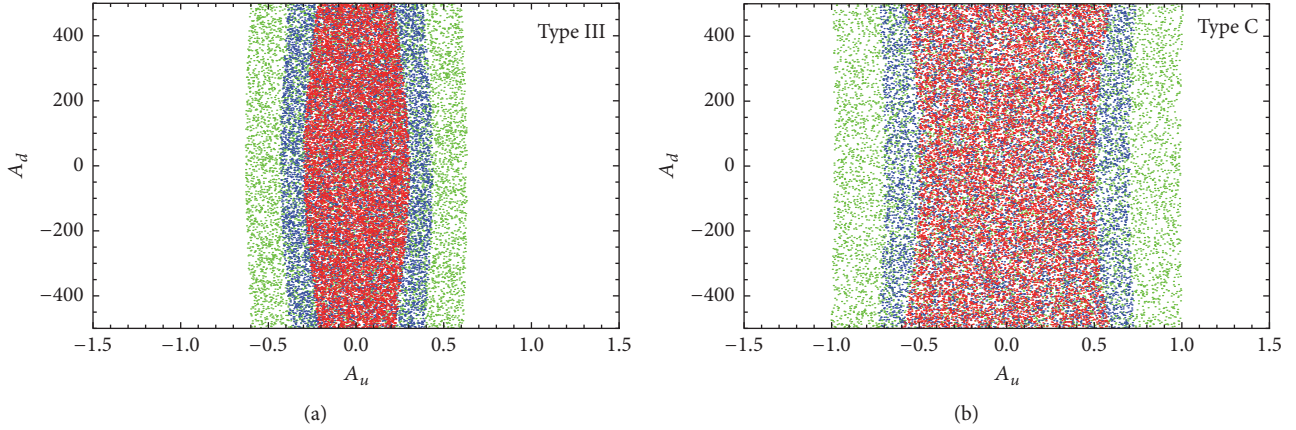


FIGURE 2: Allowed parameter spaces for A_u and A_d in the case of real coupling for type III and type C 2HDMs, under the combined constraint from Δm_K and ϵ_K . The red, blue, and green regions are obtained with m_{H^\pm} fixed at 100, 250, and 500 GeV, respectively.

From the above numerical results, we can make the following observations:

- (i) The dominant contribution to the effective Hamiltonian given by (5) comes from the operator Q^{VLL} in both type III and type C 2HDM, due to the x_s suppression in Q^{SLL} and Q^{TLL} . Furthermore, the coefficient of the $A_u A_d^*$ term in Q^{VLL} is quite small, being of order $\mathcal{O}(10^{-4})$ compared to that of the $|A_u|$ terms.
- (ii) Due to the color factor, the Wilson coefficient C^{VLL} in type C is a little bit smaller than that in type III 2HDM, and the sign of C^{SLL} in type C is also flipped relative to that in type III 2HDM.
- (iii) There exists an extra operator Q^{TLL} in type C 2HDM, and its Wilson coefficient C^{TLL} differs from that of Q^{SLL} in sign.

From the current experimental data on Δm_K and ϵ_K , one can constrain the model parameters and even distinguish the two scenarios of 2HDM with MFV. To get the plots for the allowed parameter spaces, we do as follows:

- (1) We scan the Yukawa coupling parameters A_u and A_d (also the relative phase θ for complex couplings) randomly within the ranges given by (24), with m_{H^\pm} fixed at 100, 250, and 500 GeV, respectively.
- (2) With each set of values for the model parameters, we give the theoretical prediction for Δm_K and ϵ_K , together with the corresponding uncertainty resulted from the input parameters listed in Table 1. The method of calculating the theoretical uncertainty is the same as in [34].
- (3) We select the points which lead to the theoretical predictions overlapping with the 2σ range of the experimental data.

The final allowed spaces for the model parameters are shown in Figure 2 for the real coupling and in Figure 3 for the complex coupling case, respectively.

From Figure 2, we can make the following observations for the real coupling:

- (i) In type III model, as shown in Figure 2(a), the parameter A_u is severely constrained due to the good agreement between the SM predictions and the experimental data, especially for ϵ_K ; for example, the limit $|A_u| < 0.7$ is more stringent compared to that obtained in [34] with $m_{H^\pm} = 500$ GeV. However, there is almost no constraints on A_d because of the smallness of the coefficient involving A_d , as mentioned earlier.
- (ii) In type C model, we also get strong constraint for A_u , but being looser than that in type III case, with the maximum value $|A_u| \approx 1$. The wider allowed range in type C model comes from the additional color factor. Similar to that observed in type III model, there is also almost no constraint on A_d .
- (iii) The patterns of the allowed parameter spaces of these two models are different, looking like “convex lens” for type III and like “concave lens” for type C model. This means that the allowed range for $|A_u|$ is smaller with larger $|A_d|$ for type III model, while the allowed range for $|A_u|$ in type C model can be larger with greater $|A_d|$. The reason is that the dominant contribution to the two observables Δm_K and ϵ_K comes from the operator Q^{VLL} , the Wilson coefficient of which in type C is smaller than that in type III model. Moreover, the cancellation between the Wilson coefficients Q^{SLL} and Q^{TLL} in type C model also reduces their contribution to the observables.

For the complex coupling, on the other hand, the results shown in Figure 3 imply that

- (i) in type III model, there exists a strong correlation between $|A_u|$ and $|A_u A_d^*|$, especially when $m_{H^\pm} = 100$ GeV, as shown in Figure 3(a). It is also found from Figure 3(c) that the large values of $|A_u A_d^*|$ are allowed at $\theta \approx \pm\pi/2$, due to the cancellation between the complex terms,

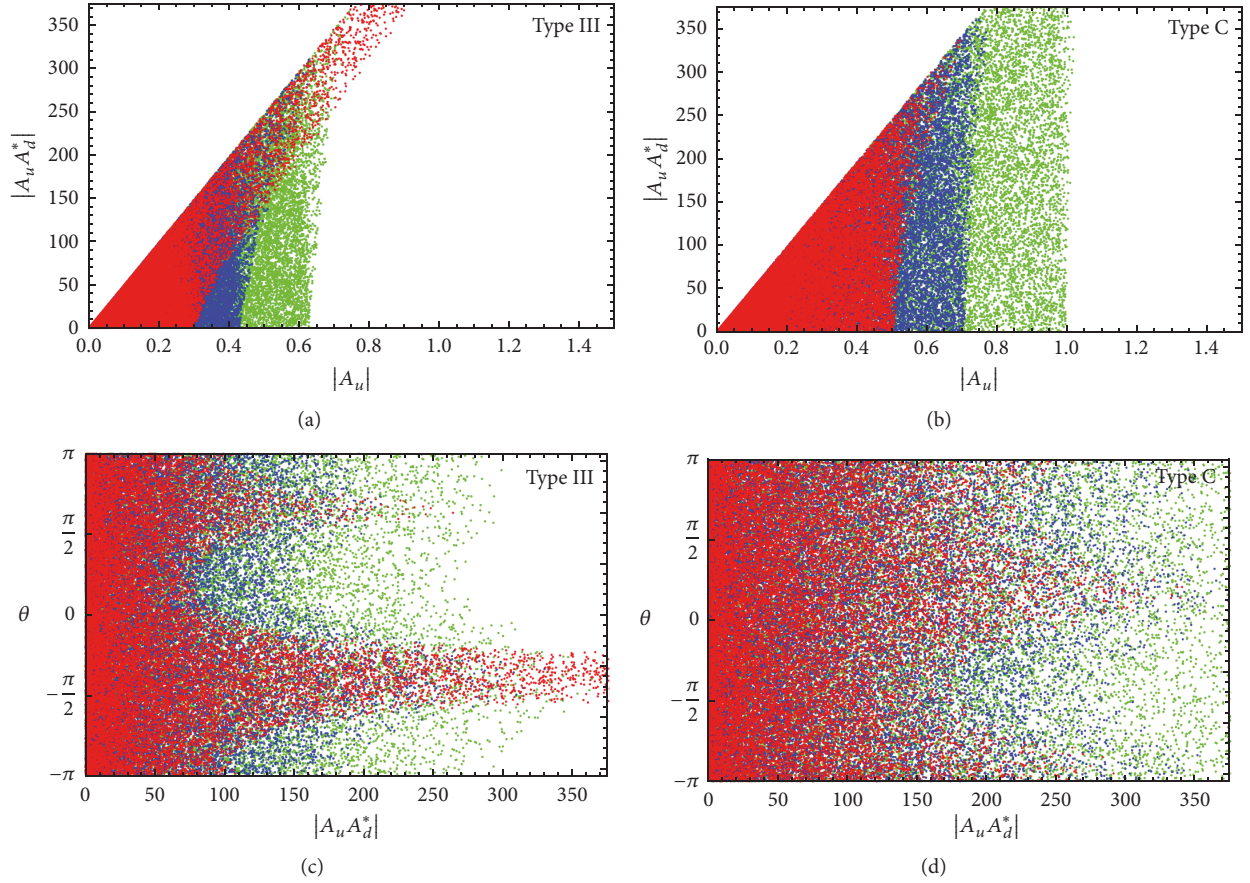


FIGURE 3: Allowed parameter spaces for $|A_u|$, $|A_u A_d^*|$, and θ in the case of complex coupling for type III and type C 2HDMs, under the combined constraint from Δm_K and ϵ_K . The exclusion region in $|A_u A_d^*|$ comes from the constraint on $|A_d|$. The other captions are the same as in Figure 2.

- (ii) in type C model, as shown in Figures 3(b) and 3(d), similar observations can also be made, except for the fact that the constraints on the couplings are now a little bit looser than that in type III model. What makes difference from type III model is that larger values of $|A_u A_d^*|$ in the $|A_u A_d^*| - \theta$ plane occur around $\theta \approx 0$ and $\pm\pi$, which are resulted from the cancellation between the complex terms.

From the above discussions, one can conclude that although type III and type C model present some significantly different behaviors under the experimental constraints from $K^0 - \bar{K}^0$ mixing, it is still hard to distinguish them from each other, especially for the real coupling case or for small $|A_d|$. This is due to the significant uncertainties of both the theoretical predictions and the experimental data. Therefore, more refined theoretical and experimental efforts are needed for a much clearer phenomenological picture.

5. Conclusion

In this paper, we have performed a complete one-loop computation of the box diagrams for the $K^0 - \bar{K}^0$ mixing, both within the SM and in type III and type C 2HDMs. It

is noted that, in order to get a gauge-independent result, the external strange-quark momentum and mass should be taken into account, which has been kept up to the second order.

Combining the latest experimental data on the $K^0 - \bar{K}^0$ mixing, we then performed a detailed phenomenological analysis of the charged-Higgs effects on this process. Our main conclusions can be summarized as follows:

- (i) The operator Q^{TLL} appears already at the matching scale in type C model, while its appearance in type III model is induced by the RG evolution effect from the high-down to the low-energy scale.
- (ii) We get strong constraint on the Yukawa coupling parameter $|A_u|$ in both the real and the complex coupling case, being even stronger than that obtained in [34], while there is almost no constraint on the other Yukawa coupling $|A_d|$.
- (iii) The allowed parameter spaces for A_u and A_d in the case of real coupling are similar for both types of models, with a wider range in type C model. If we extend the A_d range, however, the allowed region for A_u will be smaller in type III and larger in type

C model, behaving like “convex lens” and “concave lens,” respectively.

- (iv) In the case of complex coupling, the strong correlation between $|A_u|$ and $|A_u A_d^*|$ is observed, especially for $m_{H^\pm} = 100$ GeV in type III model. The relative phase between $|A_u|$ and $|A_d|$, θ , allows the large values of $|A_u A_d^*|$ at $\theta \approx \pm\pi/2$ in type III and $\theta \approx 0$ and $\pm\pi$ in type C model. This is due to the cancellation effect between the complex terms in the Wilson coefficient C^{VLL} .

Although these two types of models present some significantly different behaviors under the experimental constraints from $K^0 - \bar{K}^0$ mixing, it is still hard to distinguish one from the other, especially for the real coupling case or for small $|A_d|$. We need more refined theoretical and experimental efforts for a much clearer phenomenological picture.

Appendix

Basic Functions for $K^0 - \bar{K}^0$ Mixing

In this appendix, we collect the relevant functions during the calculation of the Wilson coefficients for $K^0 - \bar{K}^0$ mixing. Note that the notations $f(x) = \lim_{y \rightarrow x} f(x, y)$ and $f(x, x_H) = \lim_{y \rightarrow x} f(x, y, x_H)$ are applied to each function listed below.

The Inami-Lim function S_0 is given by [42]

$$S_0(x_c, x_t) = x_c x_t \left[\frac{(x_c^2 - 8x_c + 4) \ln(x_c)}{4(x_c - 1)^2(x_c - x_t)} - \frac{(x_t^2 - 8x_t + 4) \ln(x_t)}{4(x_t - 1)^2(x_c - x_t)} - \frac{3}{4(x_c - 1)(x_t - 1)} \right]. \quad (\text{A.1})$$

The functions f_i introduced in Section 3 are given explicitly as

$$\begin{aligned} f_1(x_c, x_t) &= \frac{\ln(x_t)}{12(x_t - 1)^4(x_c - x_t)^3} \left[x_c^3(x_t^4 - 9x_t^3 + 36x_t^2 - 42x_t + 12) + x_c^2 x_t(-3x_t^4 + 22x_t^3 - 87x_t^2 + 108x_t - 36) \right. \\ &\quad \left. + x_c x_t^3(15x_t^2 - 23x_t + 6) \right] + \frac{\ln(x_c)}{12(x_c - 1)^4(x_t - x_c)^3} \left[x_t^3(x_c^4 - 9x_c^3 + 36x_c^2 - 42x_c + 12) + x_t^2 x_c(-3x_c^4 + 22x_c^3 \right. \\ &\quad \left. - 87x_c^2 + 108x_c - 36) + x_t x_c^3(15x_c^2 - 23x_c + 6) \right] - \frac{1}{72(x_c - 1)^3(x_t - 1)^3(x_c - x_t)^2} \left[x_c^5(65x_t^3 - 130x_t^2 + 113x_t \right. \\ &\quad \left. - 60) + x_c^4(-118x_t^4 + 34x_t^3 + 250x_t^2 - 298x_t + 180) + x_c^3(65x_t^5 + 34x_t^4 + 66x_t^3 - 386x_t^2 + 329x_t - 180) \right. \\ &\quad \left. - 2x_c^2(65x_t^5 - 125x_t^4 + 193x_t^3 - 217x_t^2 + 90x_t - 30) + x_c x_t(113x_t^4 - 298x_t^3 + 329x_t^2 - 180x_t + 24) - 60(x_t - 1)^3 \right. \\ &\quad \left. \cdot x_t^2 \right], \\ f_2(x_c, x_t) &= \frac{x_t}{36(x_c - 1)^3(x_t - 1)^3(x_c - x_t)^2} \left[x_c^5(5x_t^2 - 22x_t + 5) + 2x_c^4(x_t^3 - x_t^2 + 35x_t - 11) + x_c^3(5x_t^4 - 2x_t^3 \right. \\ &\quad \left. - 78x_t^2 - 2x_t + 5) - 2x_c^2 x_t(11x_t^3 - 35x_t^2 + x_t - 1) + x_c(5x_t^4 - 22x_t^3 + 5x_t^2) \right] - \frac{x_c^3 x_t \ln(x_c)}{6(x_c - 1)^4(x_c - x_t)^3} \left[3x_c^2(x_t + 1) \right. \\ &\quad \left. - x_c(x_t^2 + 10x_t + 1) + 3x_t(x_t + 1) \right] - \frac{x_t^3 x_c \ln(x_t)}{6(x_t - 1)^4(x_t - x_c)^3} \left[3x_t^2(x_c + 1) - x_t(x_c^2 + 10x_c + 1) + 3x_c(x_c + 1) \right], \\ f_3(x_c, x_t) &= -\frac{1}{36(x_c - 1)^3(x_t - 1)^3(x_c - x_t)^2} \left[x_c^5(10x_t^3 - 25x_t^2 + 8x_t - 5) + x_c^4(-20x_t^4 + 25x_t^3 + 49x_t^2 - 21x_t + 15) \right. \\ &\quad \left. + x_c^3(10x_t^5 + 25x_t^4 - 102x_t^3 + 2x_t^2 + 8x_t - 15) + x_c^2(-25x_t^5 + 49x_t^4 + 2x_t^3 + 26x_t^2 - 9x_t + 5) + x_c(8x_t^5 - 21x_t^4 + 8x_t^3 \right. \\ &\quad \left. - 9x_t^2 + 2x_t) - 5(x_t - 1)^3 x_t^2 \right] - \frac{\ln(x_t)}{6(x_t - 1)^4(x_c - x_t)^3} \left[x_c^3(3x_t - 1) - x_c^2(x_t^3 + 6x_t^2 - 3x_t) + x_c(3x_t^4 - x_t^3) \right] \\ &\quad - \frac{\ln(x_c)}{6(x_c - 1)^4(x_t - x_c)^3} \left[x_t^3(3x_c - 1) - x_t^2(x_c^3 + 6x_c^2 - 3x_c) + x_t(3x_c^4 - x_c^3) \right], \end{aligned}$$

$$\begin{aligned}
f_4(x_c, x_t, x_H) &= \frac{(x_c - 4)x_c^2 x_t \ln(x_c)}{2(x_c - 1)(x_c - x_H)(x_c - x_t)} - \frac{x_c(x_t - 4)x_t^2 \ln(x_t)}{2(x_t - 1)(x_c - x_t)(x_t - x_H)} - \frac{x_c(x_H - 4)x_H x_t \ln(x_H)}{2(x_H - 1)(x_c - x_H)(x_H - x_t)} \\
&+ x_s \left\{ \frac{x_c^2 x_t \ln(x_c)}{24(x_c - 1)^3(x_c - x_H)^3(x_c - x_t)^3} \left[-3x_c^5(x_H + 2x_t - 7) + x_c^4(4x_H(4x_t - 3) + x_H^2 + 2x_t^2 + 16x_t - 23) \right. \right. \\
&- x_c^3(x_H^2(6x_t - 7) + x_H(5x_t^2 + 76x_t + 5) + 5x_t^2 + 42x_t - 12) + x_c^2(x_H^2(x_t^2 + 28x_t + 2) + 8x_H x_t(3x_t + 20) \\
&+ x_t(13x_t + 12)) - 3x_c x_H x_t(x_H(x_t + 22) + 17x_t + 20) + 12x_H x_t(x_H(x_t + 2) + x_t)] \\
&- \frac{x_c x_t^2 \ln(x_t)}{24(x_t - 1)^3(x_c - x_t)^3(x_t - x_H)^3} \left[x_c^2(x_H^2(x_t^2 - 3x_t + 12) + x_H(-5x_t^3 + 24x_t^2 - 51x_t + 12)) \right. \\
&+ x_t^2(2x_t^2 - 5x_t + 13) - 2x_c(x_H^2(3x_t^3 - 14x_t^2 + 33x_t - 12) + 2x_H x_t(-4x_t^3 + 19x_t^2 - 40x_t + 15) \\
&+ x_t^2(3x_t^3 - 8x_t^2 + 21x_t - 6)) + x_t^2(x_H^2(x_t^2 + 7x_t + 2) - x_H x_t(3x_t^2 + 12x_t + 5) + x_t(21x_t^2 - 23x_t + 12))] \\
&- \frac{x_c x_H x_t \ln(x_H)}{24(x_H - 1)^3(x_c - x_H)^3(x_H - x_t)^3} \left[x_c^2(x_H^3(6 - 5x_t) + x_H^2(2x_t^2 + 16x_t + 13) - 3x_H x_t(2x_t + 21) + x_H^4 \right. \\
&+ 12x_t(2x_t + 1)) - x_c(x_H^4(8 - 12x_t) + x_H^3(5x_t^2 + 40x_t + 41) - 4x_H^2(4x_t^2 + 39x_t + 3) + 3x_H x_t(21x_t + 16) + 3x_H^5 \\
&- 12x_t^2) + x_H^2(-3x_H^3(x_t - 6) + x_H^2(x_t^2 - 8x_t + 2) + x_H x_t(6x_t - 41) + x_t(13x_t + 12))] \left. \right\},
\end{aligned}$$

$$\begin{aligned}
g_4(x_c, x_t, x_H) &= -\frac{x_c x_t}{12(x_c - 1)^2(x_c - x_H)^2(x_H - 1)^2(x_c - x_t)^2(x_H - x_t)^2(x_t - 1)^2} \left[x_c^5((x_t^2 + 4)x_H^3 + (-13x_t^2 \right. \\
&+ 15x_t - 17)x_H^2 + (4x_t^3 - 4x_t^2 + 12x_t + 3)x_H + x_t(6x_t^2 - 14x_t + 3) - ((3x_t^2 - 2x_t + 9)x_H^4 - (2x_t^3 + 11x_t^2 - 22x_t \\
&+ 24)x_H^3 + (2x_t^4 - 16x_t^3 - 11x_t^2 + 31x_t - 21)x_H^2 + (4x_t^4 + 11x_t^3 + x_t^2 + 13x_t + 6)x_H + x_t(14x_t^3 - 23x_t^2 - 12x_t \\
&+ 6))x_c^4 + x_c^3((x_t^2 + 4)x_H^5 + (23x_t^2 - 25x_t + 17)x_H^4 + 2(x_t^4 - 32x_t^3 + 14x_t^2 + 22x_t - 35)x_H^3 + 8(2x_t^4 + x_t^3 - 4x_t^2 \\
&+ 4x_t + 2)x_H^2 + (4x_t^5 - 11x_t^4 + 8x_t^3 + 35x_t^2 - 24x_t + 3)x_H + x_t(6x_t^4 + 23x_t^3 - 72x_t^2 + 25x_t + 3)) + ((x_t^3 - 18x_t^2 \\
&+ 17x_t - 15)x_H^5 + (-3x_t^4 + 23x_t^3 - 22x_t^2 - 2x_t + 19)x_H^4 + (x_t^5 + 11x_t^4 + 28x_t^3 - 16x_t^2 - 5x_t + 21)x_H^3 - (13x_t^5 \\
&- 11x_t^4 + 32x_t^3 + 16x_t^2 - 5x_t + 15)x_H^2 - x_t(4x_t^4 + x_t^3 - 35x_t^2 + 30x_t - 15)x_H + x_t^2(-14x_t^3 + 12x_t^2 + 25x_t - 18))x_c^2 \\
&+ ((17x_t^2 - 8x_t + 6)x_H^5 + (2x_t^4 - 25x_t^3 - 2x_t^2 + 2x_t - 12)x_H^4 + (-22x_t^4 + 44x_t^3 - 5x_t^2 - 8x_t + 6)x_H^3 + x_t(15x_t^4 \\
&- 31x_t^3 + 32x_t^2 + 5x_t - 6)x_H^2 + x_t^2(12x_t^3 - 13x_t^2 - 24x_t + 15)x_H + 3(x_t - 1)^2 x_t^3)x_c + x_H x_t((4x_t^2 - 15x_t + 6)x_H^4 \\
&+ (-9x_t^3 + 17x_t^2 + 19x_t - 12)x_H^3 + (4x_t^4 + 24x_t^3 - 70x_t^2 + 21x_t + 6)x_H^2 + x_t(-17x_t^3 + 21x_t^2 + 16x_t - 15)x_H \\
&+ 3(x_t - 1)^2 x_t^2) \left. \right],
\end{aligned}$$

$$\begin{aligned}
f_5(x_c, x_t, x_H) &= -\frac{x_c \ln(x_c)}{4(x_c - 1)^2(x_c - x_H)^2(x_c - x_t)} \left[-x_c^2(6x_H + 11x_t + 6) + 2x_c(x_H(6x_t + 3) + 5x_t) + 6x_c^3 \right. \\
&- 11x_H x_t \left. \right] + \frac{x_c x_t \ln(x_t)}{4(x_t - 1)^2(x_c - x_t)(x_H - x_t)^2} \left[x_H(6x_t - 5) + (4 - 5x_t)x_t \right] \\
&+ \frac{x_c \ln(x_H)}{4(x_H - 1)^2(x_c - x_H)^2(x_H - x_t)^2} \left[x_c(-x_H^2(19x_t + 6) + x_H x_t(12x_t + 17) + 6x_H^3 - 10x_t^2) + x_H(x_H^2(20x_t + 6) \right. \\
&- x_H x_t(13x_t + 18) - 6x_H^3 + 11x_t^2) \left. \right] - \frac{x_c x_t}{4(x_c - 1)(x_H - 1)(x_t - 1)(x_c - x_H)(x_H - x_t)} \left[x_c(x_H - 2x_t + 1) + x_H x_t \right. \\
&- x_H^2 + x_t - 1 \left. \right],
\end{aligned}$$

$$\begin{aligned}
f_6(x_c, x_t, x_H) &= \frac{x_c^3 x_t \ln(x_c)}{4(x_c - x_H)^2 (x_c - x_t)} - \frac{x_c x_t^3 \ln(x_t)}{4(x_c - x_t)(x_H - x_t)^2} - \frac{x_c x_H x_t \ln(x_H)}{4(x_c - x_H)^2 (x_H - x_t)^2} [x_c(x_H - 2x_t) + x_H x_t] \\
&- \frac{x_c x_H x_t}{4(x_c - x_H)(x_H - x_t)} + x_s \left\{ \frac{x_c^3 x_t \ln(x_c)}{12(x_c - x_H)^4 (x_c - x_t)^3} [3x_c^2(x_H + x_t) - x_c(10x_H x_t + x_H^2 + x_t^2) + 3x_H x_t(x_H \right. \\
&+ x_t)] + \frac{x_c x_t^3 \ln(x_t)}{12(x_c - x_t)^3 (x_H - x_t)^4} [x_c^2(x_t - 3x_H) + x_c(10x_H x_t - 3x_H^2 - 3x_t^2) + x_H x_t(x_H - 3x_t)] \\
&+ \frac{x_c x_t \ln(x_H)}{12(x_c - x_H)^4 (x_H - x_t)^4} [-3x_c x_H^4 (x_H - 3x_t) + 3x_c^2 x_H x_t^2 (x_t - 3x_H) + x_c^3 x_t^2 (3x_H - x_t) + x_H^5 (x_H - 3x_t)] \\
&+ \frac{x_c x_t}{72(x_c - x_H)^3 (x_c - x_t)^2 (x_H - x_t)^3} [x_c^4(-22x_H x_t + 5x_H^2 + 5x_t^2) + x_c^3(70x_H^2 x_t - 2x_H x_t^2 - 22x_H^3 + 2x_t^3) \\
&+ x_c^2(-2x_H^3 x_t - 78x_H^2 x_t^2 - 2x_H x_t^3 + 5x_H^4 + 5x_t^4) + 2x_c x_H x_t(-x_H^2 x_t + 35x_H x_t^2 + x_H^3 - 11x_t^3) + x_H^2 x_t^2(-22x_H x_t \\
&+ 5x_H^2 + 5x_t^2)] \left. \right\},
\end{aligned}$$

$$\begin{aligned}
f_7(x_c, x_t, x_H) &= -\frac{x_c x_t}{12(x_c - 1)^2 (x_c - x_H)^2 (x_H - 1)^2 (x_c - x_t)^2 (x_H - x_t)^2 (x_t - 1)^2} [((x_t^2 - 3x_t + 4)x_H^3 + (-3x_t^3 \\
&+ 5x_t^2 - 8)x_H^2 + x_t(4x_t^2 - 13x_t + 15)x_H + x_t^2(3x_t - 5))x_c^5 + ((3x_t^2 - 4x_t - 3)x_H^4 + x_t(-7x_t^2 + 5x_t + 8)x_H^3 \\
&+ (10x_t^4 + x_t^3 - 16x_t^2 - 4x_t + 15)x_H^2 + x_t(-16x_t^3 + 19x_t^2 + 11x_t - 28)x_H - x_t^2(2x_t^2 + x_t - 9))x_c^4 + ((-2x_t^2 + 3x_t \\
&+ 1)x_H^5 + (6x_t^3 - 10x_t^2 + 5x_t + 5)x_H^4 + (-7x_t^4 + 8x_t^3 + 4x_t^2 - 16x_t - 13)x_H^3 + (-3x_t^5 + x_t^4 - 16x_t^3 + 28x_t^2 + 11x_t \\
&- 5)x_H^2 + x_t(4x_t^4 + 19x_t^3 - 40x_t^2 + 14x_t + 9)x_H + x_t^2(3x_t^3 - x_t^2 - 6x_t - 2))x_c^3 + ((-2x_t^3 + 6x_t^2 - 7x_t - 3)x_H^5 \\
&+ (3x_t^4 - 10x_t^3 + 8x_t^2 + x_t + 4)x_H^4 + (x_t^5 + 5x_t^4 + 4x_t^3 - 16x_t^2 + 19x_t + 3)x_H^3 + x_t(5x_t^4 - 16x_t^3 + 28x_t^2 - 40x_t - 1) \\
&\cdot x_H^2 + x_t^2(-13x_t^3 + 11x_t^2 + 14x_t - 6)x_H + x_t^3(-5x_t^2 + 9x_t - 2))x_c^2 + x_H x_t((3x_t^2 - 7x_t + 10)x_H^4 + (-4x_t^3 + 5x_t^2 \\
&+ x_t - 16)x_H^3 + (-3x_t^4 + 8x_t^3 - 16x_t^2 + 19x_t - 2)x_H^2 - x_t(4x_t^2 - 11x_t + 1)x_H + x_t^2(15x_t^2 - 28x_t + 9))x_c \\
&+ x_H^2 x_t^2((x_t - 3)x_H^3 + (-3x_t^2 + 5x_t + 4)x_H^2 + (4x_t^3 - 13x_t + 3)x_H + x_t(-8x_t^2 + 15x_t - 5))],
\end{aligned}$$

$$\begin{aligned}
g_7(x_c, x_t, x_H) &= -\frac{x_c^2 x_t \ln(x_c)}{6(x_c - 1)^3 (x_c - x_H)^3 (x_c - x_t)^3} [6x_c^6 - 3x_c^5(5x_H + 5x_t + 4) + x_c^4(5x_H(7x_t + 6) + 8x_H^2 + 7x_t^2 \\
&+ 29x_t + 5) - x_c^3(2x_H^2(9x_t + 8) + x_H(16x_t^2 + 68x_t + 13) + x_t(13x_t + 12)) + x_c^2(x_H^2(8x_t^2 + 35x_t + 7) \\
&+ x_H x_t(30x_t + 29) + 5x_t^2) - 3x_c x_H x_t(5x_H(x_t + 1) + 4x_t) + 6x_H^2 x_t^2] - \frac{x_t^2 x_c \ln(x_t)}{6(x_t - 1)^3 (x_t - x_H)^3 (x_t - x_c)^3} [6x_t^6 \\
&- 3x_t^5(5x_H + 5x_c + 4) + x_t^4(5x_H(7x_c + 6) + 8x_H^2 + 7x_c^2 + 29x_c + 5) - x_t^3(2x_H^2(9x_c + 8) + x_H(16x_c^2 + 68x_c + 13) \\
&+ x_c(13x_c + 12)) + x_t^2(x_H^2(8x_c^2 + 35x_c + 7) + x_H x_c(30x_c + 29) + 5x_c^2) - 3x_t x_H x_c(5x_H(x_c + 1) + 4x_c) \\
&+ 6x_H^2 x_c^2] + \frac{x_c x_H x_t \ln(x_H)}{6(x_H - 1)^3 (x_c - x_H)^3 (x_H - x_t)^3} [x_c^2(-x_H^3(16x_t + 15) + x_H^2(7x_t^2 + 29x_t + 5) - 3x_H x_t(4x_t + 3) \\
&+ 8x_H^4 + 3x_t^2) + x_c x_H(x_H^3(36x_t + 35) - x_H^2(16x_t^2 + 68x_t + 13) + x_H x_t(29x_t + 24) - 18x_H^4 - 9x_t^2) \\
&+ x_H^2(-18x_H^3(x_t + 1) + x_H^2(8x_t^2 + 35x_t + 7) - x_H x_t(15x_t + 13) + 9x_H^4 + 5x_t^2)],
\end{aligned}$$

$$\begin{aligned}
f_8(x_c, x_t, x_H) &= \frac{x_c x_t}{4(x_c - 1)(x_H - 1)(x_t - 1)(x_c - x_H)(x_H - x_t)} [x_H(x_c(x_t - 2) - 2x_t + 1) + x_c x_t + x_H^2] \\
&- \frac{x_c^2 \ln(x_c)}{4(x_c - 1)^2(x_c - x_H)^2(x_c - x_t)} [-x_c^2(9x_H + 16x_t + 9) + x_c(x_H(17x_t + 9) + 15x_t) + 9x_c^3 - 16x_H x_t] \\
&+ \frac{x_c x_t^2 \ln(x_t)}{4(x_t - 1)^2(x_c - x_t)(x_H - x_t)^2} [x_H(8x_t - 7) + (6 - 7x_t)x_t] \\
&+ \frac{x_c x_H \ln(x_H)}{4(x_H - 1)^2(x_c - x_H)^2(x_H - x_t)^2} [x_c(-x_H^2(26x_t + 9) + 8x_H x_t(2x_t + 3) + 9x_H^3 - 14x_t^2) + x_H(9x_H^2(3x_t + 1) \\
&- x_H x_t(17x_t + 25) - 9x_H^3 + 15x_t^2)], \\
f_9(x_c, x_t, x_H) &= -\frac{x_c^3 x_t \ln(x_c)}{6(x_c - x_H)^4(x_c - x_t)^3} [3x_c^2(x_H + x_t) - x_c(10x_H x_t + x_H^2 + x_t^2) + 3x_H x_t(x_H + x_t)] \\
&- \frac{x_c x_t^3 \ln(x_t)}{6(x_c - x_t)^3(x_H - x_t)^4} [x_c^2(x_t - 3x_H) + x_c(10x_H x_t - 3x_H^2 - 3x_t^2) + x_H x_t(x_H - 3x_t)] \\
&+ \frac{x_c x_t \ln(x_H)}{6(x_c - x_H)^4(x_H - x_t)^4} [3x_c x_H^4(x_H - 3x_t) + 3x_c^2 x_H x_t^2(3x_H - x_t) + x_c^3 x_t^2(x_t - 3x_H) + x_H^5(3x_t - x_H)] \\
&- \frac{x_c x_t}{36(x_c - x_H)^3(x_c - x_t)^2(x_H - x_t)^3} [x_c^4(-22x_H x_t + 5x_H^2 + 5x_t^2) + x_c^3(70x_H^2 x_t - 2x_H x_t^2 - 22x_H^3 + 2x_t^3) \\
&+ x_c^2(-2x_H^3 x_t - 78x_H^2 x_t^2 - 2x_H x_t^3 + 5x_H^4 + 5x_t^4) + 2x_c x_H x_t(-x_H^2 x_t + 35x_H x_t^2 + x_H^3 - 11x_t^3) + x_H^2 x_t^2(-22x_H x_t \\
&+ 5x_H^2 + 5x_t^2)], \\
f_{10}(x_c, x_t, x_H) &= \frac{x_c^2 x_t \ln(x_c)}{(x_c - x_H)^2(x_c - x_t)} - \frac{x_c x_t^2 \ln(x_t)}{(x_c - x_t)(x_H - x_t)^2} + \frac{x_c x_t \ln(x_H)}{(x_c - x_H)^2(x_H - x_t)^2} [x_c x_t - x_H^2] \\
&- \frac{x_c x_t}{(x_c - x_H)(x_H - x_t)}.
\end{aligned} \tag{A.2}$$

Conflicts of Interest

The authors declare that they have no conflicts of interest.

Acknowledgments

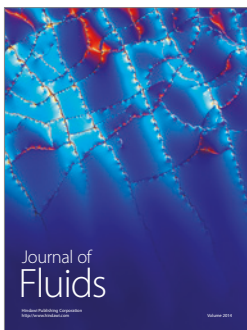
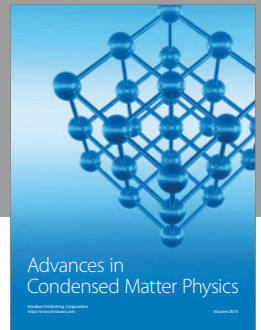
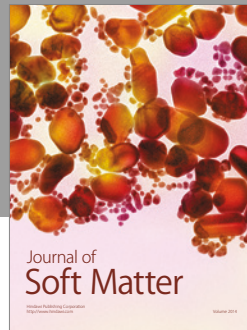
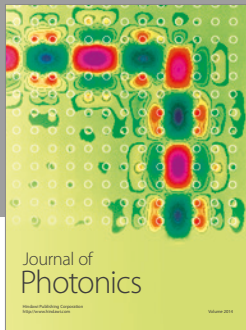
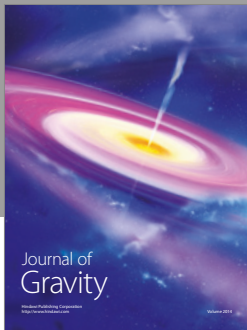
The work is supported by the National Natural Science Foundation of China (NSFC) under Contract nos. 11675061 and 11435003. Xin Zhang is supported by the CCNU-QLPL Innovation Fund (QLPL2015P01).

References

- [1] ATLAS Collaboration, "Observation of a new particle in the search for the standard model higgs boson with the ATLAS detector at the LHC," *Physics Letters B*, vol. 716, no. 1, pp. 1–29, 2012.
- [2] CMS Collaboration, "Observation of a new boson at a mass of 125 GeV with the CMS experiment at the LHC," *Physics Letters B*, vol. 716, no. 1, pp. 30–61, 2012.
- [3] M. S. Carena and H. E. Haber, "Higgs boson theory and phenomenology," *Progress in Particle and Nuclear Physics*, vol. 50, no. 1, pp. 63–152, 2003.
- [4] M. Trodden, "Electroweak baryogenesis: a brief review," in *Proceedings of the 33rd Rencontres de Moriond 98 Electroweak Interactions and Unified Theories: Les racs*, vol. 71, pp. 1463–1500, 1998.
- [5] S. Dimopoulos and L. Susskind, "Baryon asymmetry in the very early universe," *Physics Letters B*, vol. 81, no. 3-4, pp. 416–418, 1979.
- [6] J. M. Cline, "Baryogenesis," in *Proceedings of the Les Houches Summer School - Session 86: Particle Physics and Cosmology: The Fabric of Spacetime Les Houches*, vol. 86, 2006.
- [7] T. D. Lee, "A theory of spontaneous t violation," *Physical Review D*, vol. 8, no. 4, Article ID 1226, pp. 1226–1239, 1973.
- [8] N. Cabibbo, "Unitary symmetry and leptonic decays," *Physical Review Letters*, vol. 10, no. 12, pp. 531–533, 1963.

- [9] M. Kobayashi and T. Maskawa, "CP violation in the renormalizable theory of weak interaction," *Progress of Theoretical Physics*, vol. 49, pp. 652–657, 1973.
- [10] S. L. Glashow, J. Iliopoulos, and L. Maiani, "Weak interactions with lepton-hadron symmetry," *Physical Review D*, vol. 2, no. 7, pp. 1285–1292, 1970.
- [11] S. L. Glashow and S. Weinberg, "Natural conservation laws for neutral currents," *Physical Review D*, vol. 15, no. 7, pp. 1958–1965, 1977.
- [12] A. J. Buras, P. Gambino, M. Gorbahn, S. Jäger, and L. Silvestrini, "Universal unitarity triangle and physics beyond the standard model," *Physics Letters, Section B: Nuclear, Elementary Particle and High-Energy Physics*, vol. 500, no. 1-2, pp. 161–167, 2001.
- [13] A. J. Buras, M. V. Carlucci, S. Gori, and G. Isidori, "Higgs-mediated FCNCs: natural flavour conservation vs. minimal flavour violation," *Journal of High Energy Physics*, vol. 2010, no. 10, article no. 009, 2010.
- [14] G. D'Ambrosio, G. F. Giudice, G. Isidori, and A. Strumia, "Minimal flavour violation: an effective field theory approach," *Nuclear Physics B*, vol. 645, no. 3, pp. 155–187, 2002.
- [15] E. Cerveró and J.-M. Gérard, "Minimal violation of flavour and custodial symmetries in a vectophobic two-Higgs-doublet-model," *Physics Letters, Section B: Nuclear, Elementary Particle and High-Energy Physics*, vol. 712, no. 3, pp. 255–260, 2012.
- [16] A. M. Hadeed and B. Holdom, "Remnant family symmetries: a case for D0-D0mixing," *Physics Letters B*, vol. 159, no. 4-6, pp. 379–384, 1985.
- [17] G. Branco, W. Grimus, and L. Lavoura, "Relating the scalar flavour-changing neutral couplings to the CKM matrix," *Physics Letters B*, vol. 380, no. 1-2, pp. 119–126, 1996.
- [18] G. Cvetič, S. S. Hwang, and C. S. Kim, "Higgs-mediated flavor-changing neutral currents in the general framework with two Higgs doublets: An RGE analysis," *Physical Review D - Particles, Fields, Gravitation and Cosmology*, vol. 58, no. 11, pp. 1.16003E6–1.16004E7, 1998.
- [19] G. Bhattacharyya, D. Das, and A. Kundu, "Feasibility of light scalars in a class of two-Higgs-doublet models and their decay signatures," *Physical Review D - Particles, Fields, Gravitation and Cosmology*, vol. 89, no. 9, Article ID 095029, 2014.
- [20] M. D. Campos, D. Cogollo, M. Lindner, T. Melo, F. S. Queiroz, and W. Rodejohann, *Neutrino Masses and Absence of Flavor Changing Interactions in the 2HDM from Gauge Principles*.
- [21] G. Branco, P. Ferreira, L. Lavoura, M. Rebelo, M. Sher, and J. P. Silva, "Theory and phenomenology of two-Higgs-doublet models," *Physics Reports*, vol. 516, no. 1-2, pp. 1–102, 2012.
- [22] J. F. Gunion, H. E. Haber, G. L. Kane, and S. Dawson, "The higgs hunters guide," *Frontier of Physics*, vol. 80, pp. 1–404, 2000.
- [23] S. Davidson and H. E. Haber, "Basis-independent methods for the two-Higgs-doublet model," *Physical Review D*, vol. 72, no. 9, Article ID 099902, 2005.
- [24] A. V. Manohar and M. B. Wise, "Flavor changing neutral currents, an extended scalar sector, and the Higgs production rate at the CERN Large Hadron Collider," *Physical Review D - Particles, Fields, Gravitation and Cosmology*, vol. 74, no. 3, Article ID 035009, 2006.
- [25] G. Degrandi and P. Slavich, "QCD corrections in two-Higgs-doublet extensions of the standard model with minimal flavor violation," *Physical Review D-Particles, Fields, Gravitation and Cosmology*, vol. 81, no. 7, Article ID 075001, 2010.
- [26] A. Pich and P. Tuzón, "Yukawa alignment in the two-Higgs-doublet model," *Physical Review D - Particles, Fields, Gravitation and Cosmology*, vol. 80, no. 9, Article ID 091702, 2009.
- [27] M. Jung, A. Pich, and P. Tuzón, "Charged-Higgs phenomenology in the aligned two-Higgs-doublet model," *Journal of High Energy Physics*, vol. 2010, no. 11, 2010.
- [28] X.-Q. Li, Y.-D. Yang, and X.-B. Yuan, "Exclusive radiative B-meson decays within minimal flavor-violating two-Higgs-doublet models," *Physical Review D - Particles, Fields, Gravitation and Cosmology*, vol. 89, no. 5, Article ID 054024, 2014.
- [29] M. I. Gresham and M. B. Wise, "Color octet scalar production at the CERN LHC," *Physical Review D - Particles, Fields, Gravitation and Cosmology*, vol. 76, no. 7, Article ID 075003, 2007.
- [30] A. Idilbi, C. Kim, and T. Mehen, "Factorization and resummation for single color-octet scalar production at the LHC," *Physical Review D - Particles, Fields, Gravitation and Cosmology*, vol. 79, no. 11, Article ID 114016, 2009.
- [31] R. Bonciani, G. Degrandi, and A. Vicini, "Scalar particle contribution to Higgs production via gluon fusion at NLO," *Journal of High Energy Physics*, vol. 2007, no. 11, article 095, 2007.
- [32] C. P. Burgess, M. Trott, and S. Zuberi, "Light octet scalars, a heavy Higgs and minimal flavour violation," *Journal of High Energy Physics*, vol. 2009, no. 9, article 082, 2009.
- [33] A. Crivellin, C. Greub, and A. Kokulu, "Flavor-phenomenology of two-Higgs-doublet models with generic Yukawa structure," *Physical Review D - Particles, Fields, Gravitation and Cosmology*, vol. 87, no. 9, Article ID 094031, 2013.
- [34] Q. Chang, P.-F. Li, and X.-Q. Li, "Bs0-Bs0 mixing within minimal flavor-violating two-Higgs-doublet models," *The European Physical Journal C: Particles and Fields*, vol. 75, no. 12, p. 594, 2015.
- [35] J. P. Ellis, "TikZ-feynman: feynman diagrams with TikZ," *Computer Physics Communications*, vol. 210, pp. 103–123, 2017.
- [36] J. Urban, F. Krauss, and G. Soff, "Influence of external momenta in K0 anti-K0 and B0 anti-B0 mixing," *Journal of Physics G: Nuclear and Particle Physics*, vol. 23, pp. L25–L31, 1997.
- [37] A. J. Buras, S. Jäger, and J. Ö. Urban, "Master formulae for $\Delta F=2$ NLO-QCD factors in the Standard Model and beyond," *Nuclear Physics B*, vol. 605, no. 1-3, pp. 600–624, 2001.
- [38] A. J. Buras, D. Guadagnoli, and G. Isidori, "On ϵ_K beyond lowest order in the operator product expansion," *Physics Letters, Section B: Nuclear, Elementary Particle and High-Energy Physics*, vol. 688, no. 4-5, pp. 309–313, 2010.
- [39] J.-M. Gérard, C. Smith, and S. Trine, "Radiative kaon decays and the penguin contribution to the $\Delta I = 1/2$ rule," *Nuclear Physics B*, vol. 730, no. 1-2, pp. 1–36, 2005.
- [40] Z. Ligeti and F. Sala, "A new look at the theory uncertainty of ϵ_K ," *Journal of High Energy Physics*, vol. 2016, no. 9, 2016.
- [41] FLAG Working Group, "Review of lattice results concerning low-energy particle physics," *The European Physical Journal C: Particles and Fields*, vol. 77, no. 2, p. 112, 2017.
- [42] T. Inami and C. S. Lim, "Effects of Superheavy Quarks and Leptons in Low-Energy Weak Processes $k(L) \rightarrow \mu$ anti- μ , $K^+ \rightarrow \pi^+$ Neutrino anti-neutrino and $K^0 \leftrightarrow$ anti- K^0 ," *Progress of Theoretical Physics*, vol. 65, no. 1, pp. 297–314, 1981.
- [43] A. J. Buras, M. Jamin, and P. H. Weisz, "Leading and next-to-leading QCD corrections to ϵ -parameter and B0B0 mixing in the presence of a heavy top quark," *Nuclear Physics, Section B*, vol. 347, no. 3, pp. 491–536, 1990.
- [44] J. Brod and M. Gorbahn, " ϵ_K at next-to-next-to-leading order: The charm-top-quark contribution," *Physical Review D - Particles, Fields, Gravitation and Cosmology*, vol. 82, no. 9, Article ID 094026, 2010.

- [45] J. Brod and M. Gorbahn, “Next-to-next-to-leading-order charm-quark contribution to the CP violation parameter μ_K and Δm_K ,” *Physical Review Letters*, vol. 108, no. 12, Article ID 121801, 2012.
- [46] C. Bobeth, A. J. Buras, A. Celis, and M. Jung, “Patterns of flavour violation in models with vector-like quarks,” *Journal of High Energy Physics*, vol. 2017, no. 4, 2017.
- [47] Particle Data Group, “Review of particle physics,” *Chinese Physics C*, vol. 40, no. 10, p. 100001, 2016.
- [48] B. J. Choi et al., “Kaon BSM B-parameters using improved staggered fermions from $N_f = 2 + 1$ unquenched QCD,” *Physical Review D*, vol. 93, no. 1, Article ID 014511, 2016.
- [49] K. G. Chetyrkin, J. H. Kuhn, and M. Steinhauser, “RunDec: a mathematica package for running and decoupling of the strong coupling and quark masses,” *Computer Physics Communications*, vol. 133, no. 1, pp. 43–65, 2000.
- [50] ALEPH Collaboration, DELPHI Collaboration, L3 Collaboration, OPAL Collaboration, and LEP Collaboration, “Search for charged Higgs bosons: combined results using LEP data,” *The European Physical Journal C*, vol. 73, no. 2463, 2013.
- [51] P. Gutierrez, “Review of charged higgs searches at the tevatron,” *PoS CHARGED*, vol. 10, 2010.
- [52] ATLAS Collaboration, “Search for a charged higgs boson produced in the vector-boson fusion mode with decay $H^\pm \rightarrow W^\pm Z$ using pp collisions at $s = 8$ TeV with the ATLAS Experiment,” *Physical Review Letters*, vol. 114, no. 23, Article ID 231801, 2015.
- [53] CMS Collaboration, “Search for a charged Higgs boson in pp collisions at $s = 8$ TeV,” *The Journal of High Energy Physics*, vol. 1511, p. 018, 2015.
- [54] A. Hayreter and G. Valencia, “LHC constraints on color octet scalars,” *arXiv: 1703.04164*.
- [55] A. Arbey, F. Mahmoudi, O. Stal, and T. Stefaniak, “Status of the charged higgs boson in two higgs doublet models,” *High Energy Physics-Phenomenology*, 35 pages, 2017.



Hindawi

Submit your manuscripts at
<https://www.hindawi.com>

